

Interaction fields based on incompatibility tensor in field theory of plasticity-Part II: Application-

Tadashi Hasebe*

Kobe University, Rokkodai, Nada, Kobe 657-8501, Japan

(Received March 23, 2008, Accepted August 15, 2008)

Abstract. The theoretical framework of the interaction fields for multiple scales based on field theory is applied to one-dimensional problem mimicking dislocation substructure sensitive intra-granular inhomogeneity evolution under fatigue of Cu-added steels. Three distinct scale levels corresponding respectively to the orders of (A)dislocation substructures, (B)grain size and (C)grain aggregates are set-up based on FE-RKPM (reproducing kernel particle method) based interpolated strain distribution to obtain the incompatibility term in the interaction field. Comparisons between analytical conditions with and without the interaction, and that among different cell size in the scale A are simulated. The effect of interaction field on the B-scale field evolution is extensively examined. Finer and larger fluctuation is demonstrated to be obtained by taking account of the field interactions. Finer cell size exhibits larger field fluctuation whereas the coarse cell size yields negligible interaction effects.

Keywords: multiscale modeling; crystal plasticity; field theory; differential geometry; non-Riemannian plasticity.

1. Introduction

Materials can be viewed as an example of complex systems, where non-linear interactions among multiple scales do exist together with feedback loops among them, making it more than the some of its parts far beyond “reductionistic” perspective (Hasebe 2008, Phillips 2001). To model such complexities, at least we need to deal with “interactions” among plural scales, together with the evolutionary aspects of the individual inhomogeneities. Fortunately, our experiences have shown that each scale seems to have its own evolutionary rule or the like for the inhomogeneous fields based on rather distinct physical and geometrical origins. Let us take examples by choosing three important scale levels in polycrystalline plasticity of metallic materials in terms of inhomogeneous field evolutions, i.e., the scales of (A) dislocation substructures, (B) grain size and (C) grain aggregates (Hasebe 2004a, 2004b, 2006).

The scale A, for dislocation substructures, collective effects of interacting dislocations at high density in the sense of statistical mechanics is responsible for the dislocation clustering into patterns, while the long-range internal stress field evolving concurrently tends to determine the resultant morphology and size of the pattern, especially in the case of cellular structures (Hasebe 2006). The

* E-mail: hasebe@mech.kobe-u.ac.jp

scale B, on the other hand, the field evolution in here is mainly attributed to the geometrical constraints imposed by the external load together with those from the surrounding grains, which is describable by the continuum mechanics-based formalism (Aoyagi and Hasebe 2007). It should be noted that the morphology of the substructures to be evolved is essentially dominated by the crystallographic information except the case of shear bands, which are rather influenced by macroscopic stress states and thus can penetrate plural crystal grains not always being terminated at the grain boundaries. Field evolutions in the scale C are attributed, to a large extent, to collective behaviors of crystal grains composing the polycrystalline aggregate, in terms of role-sharing and duality (Hasebe (2004a, 2004b, 2006)). In this case, different from dislocations in the scale A, the statistical mechanics framework cannot be directly applied because of the non-distinguishability of the crystal grains, each of which has its own shape, size and crystallographic characters.

The above-mentioned rather distinct mechanisms for individual-scale field evolutions have encouraged the simple “information-passage” type modeling perspectives, which are more or less effective in many situations. But questions arise: What are the interactions like and when and how they are activated? Here is the key for us to go beyond the “reductionistic” perspectives, promoting the conventional multiscale modeling to grow into practically feasible stages. A theoretical framework for describing the inter-field correlations among multiple scales was developed and implemented into a crystalline plasticity-based constitutive model in Part I of this study (Hasebe 2008). The output there can provide us with a new standpoint to examine multiscale crystalline plasticity problems in the light of “interaction” among plural scales. In Part II, a prer, minary simulation on a three scale problem is given to show what the interactions are like, together with some potentially tractable future scopes based on it. A FE simulation result based on crystalline plasticity (Aoyagi *et al.* 2008) is used as the initial input for the present simulation, assuming three scales of great significance in polycrystalline plasticity, i.e., the scales A, B and C, exemplified above.

2. Analytical model and procedure

Fig. 1 shows the one-dimensional strain distribution used as the initial condition in the present study. The strain distribution has been obtained in a finite element (FE) analysis on a multi-grained model (Aoyagi *et al.* 2008), where the plots indicate the FEM results, while the line approximated based on the reproducing kernel particle method (RKPM) (Liu *et al.* 1995, Chen *et al.* 1996). Corresponding contour diagrams of $F(\eta^{(a)})$ are shown in the inset. Three scales, A, B and C, chosen here are indicated in Fig. 2, where the number of modulations in the central grain along the transverse cross section is plotted against the evaluation range (size) of the second derivative. For the scale A, the effective cell size model is used to evaluate the strain distribution and its derivatives therein, assuming the periodicity commensurate with $d_{cell}(\mathbf{x})$, whose detailed treatments are given below.

In the following section, we will firstly derives a general expressions for the three scale interaction field with the effective cell size-based A-scale field applicable to full 3D situations. Secondly, its reduced version to the 1D problem to be treated here will be given.

2.1 General expressions for three-scale problem

To evaluate the distortion and strain distributions in the scale A, we virtually assume the

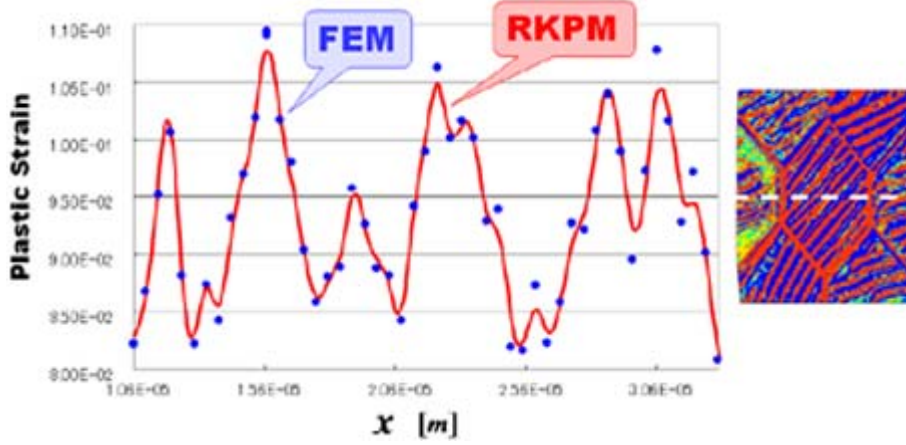


Fig. 1 Plastic strain/distortion distribution obtained in field theory-based FEM analysis and interpolated by RKPM employed in 1D-interaction field simulation

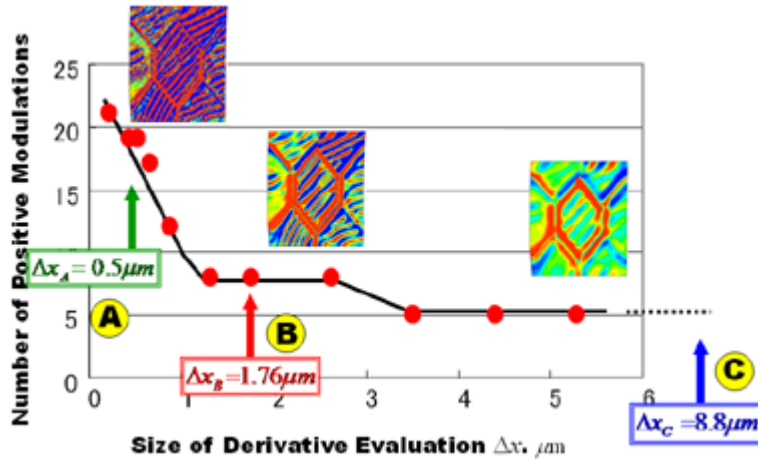


Fig. 2 Variation of number of modulations in incompatibility distribution with evaluation size of derivative, together with three scales, A, B and C, chosen for field interaction analysis

following sinusoidal form with a periodicity corresponding to the effective cell size $d_{cell}(\mathbf{x})$ in a point-wise manner as schematically depicted in Fig. 3. Tensorial versions of the A-scale distortion and strain are assumed to be given as,

$$\beta_{ij}^{eA} = \beta_{ij}^{e-cell} \sin\left(\frac{2\pi}{d_{cell}^{ij}(\mathbf{x})} \cdot \mathbf{x}^A\right) \text{ and } \varepsilon_{ij}^{eA} = (\beta_{ij}^{eA})_{sym} \quad (1)$$

where \mathbf{x}^A represents A-scale coordinates whose values are given randomly, while β_{ij}^{e-cell} and $\varepsilon_{ij}^{e-cell}$ are the amplitudes of the cell size-order elastic distortion and the corresponding elastic strain fluctuations. Here, $d_{cell}^{ij}(\mathbf{x})$ is to be evaluated from the effective cell size for each slip system, i.e., $d_{cell}^{(\alpha)}(\mathbf{x})$ by multiplying a direction tensor and taking summation over all the slip systems considered, namely,

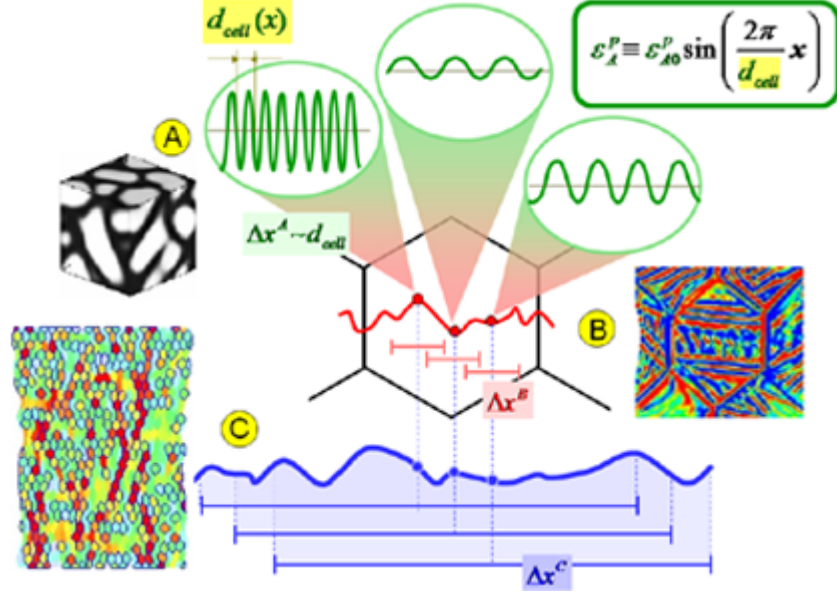


Fig. 3 Schematic drawing for treatment of A scale in the present simulation

$$d_{cell}^{ij}(\mathbf{x}) \equiv \sum_{\alpha}^N (s_i^{(\alpha)} m_j^{(\alpha)}) d_{cell}^{(\alpha)}(\mathbf{x}) \quad (2)$$

where, $s_i^{(\alpha)}$ and $m_j^{(\alpha)}$ indicate unit vectors in the slip direction and slip plane normal for the (α) slip system, respectively. The above equation was obtained by equating,

$$\tau^{(\alpha)} = K\mu \frac{b}{d_{cell}^{(\alpha)}(\mathbf{x})} \quad (3)$$

and

$$\tau^{(\alpha)} = P_{ij}^{(\alpha)} \sigma_{ij}^{cell} = P_{ij}^{(\alpha)} (D_{ijkl}^e \epsilon_{kl}^{e-cell}) \quad (4)$$

Here, $P_{ij}^{(\alpha)}$ is the Schmid tensor defined by $P_{ij}^{(\alpha)} = (s_i^{(\alpha)} m_j^{(\alpha)})$ sym. The corresponding elastic distortion and strain amplitudes β_{ij}^{e-cell} , and ϵ_{ij}^{e-cell} appear in Eq. (1) are estimated based on linear elasticity, together with the similitude relationship for the resolved shear stress with the reciprocal of $d_{cell}^{(\alpha)}(\mathbf{x})$, as,

$$\beta_{ij}^{e-cell} = \epsilon_{ij}^{e-cell} = (D_{mnij}^e P_{mn}^{(\alpha)})^{-1} \cdot K\mu \frac{b}{d_{cell}^{(\alpha)}(\mathbf{x})} \quad (5)$$

Note that the above-assumed sinusoidal form of the distortion or strain itself does not correspond directly to the A-scale fluctuations but its derivatives at each point do characterize them, i.e., as the dislocation density and incompatibility fields.

By using distortion or strain tensor expressed by Eq. (1) for the A scale, we calculate explicitly the dislocation density and incompatibility tensors, respectively, as,

$$\begin{aligned}\alpha_{ij}^A &= \epsilon_{ikl} \partial_k^A \beta_{lj}^{eA} \\ &= \epsilon_{ikl} \partial_k^A \beta_{lj}^{e-cell} \sin\left(\frac{2\pi}{d_{cell}^{ij}} x^A\right) = \epsilon_{ikl} \left\{ \frac{2\pi \beta_{ij}^{e-cell}}{d_{cell}^{ij}} \cos\left(\frac{2\pi}{d_{cell}^{ij}} x^A\right) \right\}\end{aligned}\quad (6)$$

and

$$\begin{aligned}\eta_{ij}^A &= -(\epsilon_{ikl} \partial_k^A \alpha_{jl}^A)_{sym} \\ &= -\epsilon_{ikl} \epsilon_{jmn} \partial_k^A \partial_m^A \mathcal{E}_{ln}^{eA} = -\epsilon_{ikl} \epsilon_{jmn} \partial_k^A \partial_m^A \mathcal{E}_{ln}^{e-cell} \sin\left(\frac{2\pi}{d_{cell}^{jn}} x^A\right) \\ &= -\left\{ \epsilon_{ikl} \left(\frac{2\pi}{d_{cell}^{jl}}\right)^2 \mathcal{E}_{jl}^{e-cell} \sin\left(\frac{2\pi}{d_{cell}^{jl}} x^A\right) \right\}_{sym}\end{aligned}\quad (7)$$

For scales B and C, we will conduct direct evaluation of the derivatives, i.e.,

$$\begin{aligned}\alpha_{ij}^B &= -\epsilon_{ikl} \partial_k^B \beta_{lj}^{pB} \\ \eta_{ij}^B &= -(\epsilon_{ikl} \partial_k^B \alpha_{jl}^B)_{sym} = \epsilon_{ikl} \epsilon_{jmn} \partial_k^B \partial_m^B \mathcal{E}_{ln}^{pB}\end{aligned}\quad (8)$$

and

$$\begin{aligned}\alpha_{ij}^C &= -\epsilon_{ikl} \partial_k^C \beta_{lj}^{pC} \\ \eta_{ij}^C &= -(\epsilon_{ikl} \partial_k^C \alpha_{jl}^C)_{sym} = \epsilon_{ikl} \epsilon_{jmn} \partial_k^C \partial_m^C \mathcal{E}_{ln}^{pC}\end{aligned}\quad (9)$$

For the interaction terms, e.g., between scales A and B,

$$\begin{aligned}\eta_{ij}^{BA} &= \epsilon_{ikl} \epsilon_{jmn} \partial_k^B \partial_m^A \mathcal{E}_{ln}^{eA} = -\epsilon_{ikl} \epsilon_{jmn} \partial_k^B \partial_m^A \mathcal{E}_{ln}^{e-cell} \sin\left(\frac{2\pi}{d_{cell}^{ln}} x^A\right) = -(\epsilon_{ikl} \partial_k^B \alpha_{jl}^A)_{sym} \\ &= -\left\{ \epsilon_{ikl} \partial_k^B \frac{2\pi \mathcal{E}_{jl}^{e-cell}}{d_{cell}^{jl}} \cos\left(\frac{2\pi}{d_{cell}^{jl}} x^A\right) \right\}_{sym}\end{aligned}\quad (10)$$

$$\eta_{ij}^{AB} = \epsilon_{ikl} \epsilon_{jmn} \partial_k^A \partial_m^B \mathcal{E}_{ln}^{pB} = -(\epsilon_{ikl} \partial_k^A \alpha_{jl}^B)_{sym}\quad (11)$$

It should be noted that, in the second interaction component η_{AB}^{int} , the further differentiation of α_{jl}^B with respect to the A-scale coordinates, which has been virtually introduced, cannot be explicitly performed. To this end, we tentatively assume a locally (point-wise) sinusoidal variation of α_{jl}^B with a periodicity corresponding to the evaluation range of the differentiation in the B-scale Δx^B plus its additional finer fluctuation with respect to the A scale in the present paper, i.e.,

$$\alpha_{jl}^B(x^A) \approx \alpha_{jl}^B \sin\left(\frac{2\pi}{\Delta x^B} x^A\right) + \delta \alpha_{jl}^B(x^A) \approx \alpha_{jl}^B \sin\left(\frac{2\pi}{\Delta x^B} x^A\right) + \alpha_{jl}^A\quad (12)$$

Assuming the A-scale fluctuation $\delta \alpha_{ij}^B(x^A)$ in the above to be commensurate with α_{ij}^A , i.e., $\delta \alpha_{ij}^B(x^A) \approx \alpha_{ij}^A$, we finally have for Eq. (11),

$$\begin{aligned}
\eta_{ij}^{AB} &\approx \left\{ \epsilon_{ikl} \partial_k^A \alpha_{jl}^B \sin\left(\frac{2\pi}{\Delta x^B} x^A\right) + \epsilon_{ikl} \partial_k^A \alpha_{jl}^A \right\}_{sym} \\
&= -\frac{2\pi(\epsilon_{ikl} \alpha_{jl}^B)}{\Delta x^B} \cos\left(\frac{2\pi}{\Delta x^B} x^A\right) + \eta_{ij}^A
\end{aligned} \tag{11a}$$

Similarly, for the interaction between scales C and A, we have,

$$\begin{aligned}
\eta_{ij}^{CA} &= -\epsilon_{ikl} \epsilon_{jmn} \partial_k^C \partial_m^A \epsilon_{ln}^{eA} = -\epsilon_{ikl} \epsilon_{jmn} \partial_k^C \partial_m^A \epsilon_{ln}^{e-cell} \sin\left(\frac{2\pi}{d_{cell}^{ln}} x^A\right) = -(\epsilon_{ikl} \partial_k^C \alpha_{jl}^A)_{sym} \\
&= \left\{ \epsilon_{ikl} \partial_k^C \frac{2\pi \epsilon_{jl}^{e-cell}}{d_{cell}^{jl}} \cos\left(\frac{2\pi}{d_{cell}^{jl}} x^A\right) \right\}_{sym}
\end{aligned} \tag{13}$$

$$\begin{aligned}
\eta_{ij}^{AC} &= \epsilon_{ikl} \epsilon_{jmn} \partial_k^A \partial_m^C \epsilon_{ln}^{pC} = -(\epsilon_{ikl} \partial_k^A \alpha_{jl}^C)_{sym} \\
&\approx \left\{ \epsilon_{ikl} \partial_k^A \alpha_{jl}^C \sin\left(\frac{2\pi}{\Delta x^C} x^C\right) + \epsilon_{ikl} \partial_k^A \alpha_{jl}^A \right\}_{sym} \\
&= -\frac{2\pi(\epsilon_{ikl} \alpha_{jl}^C)}{\Delta x^C} \cos\left(\frac{2\pi}{\Delta x^C} x^A\right) + \eta_{ij}^A
\end{aligned} \tag{14}$$

For another interaction between scales B and C, we directly calculate via,

$$\eta_{ij}^{BC} = \epsilon_{ikl} \epsilon_{jmn} \partial_k^B \partial_m^C \epsilon_{ln}^{pC} \tag{15}$$

$$\eta_{ij}^{CB} = \epsilon_{ikl} \epsilon_{jmn} \partial_k^C \partial_m^B \epsilon_{ln}^{pB} \tag{16}$$

Combining Eqs. (6)-(16) altogether, finally we have the total incompatibility tensor for the interaction field. The total dislocation density and incompatibility tensors in their direct as well as index notations are given by,

$$\tilde{\alpha}_{ij} = e_{BC}^{-1} \alpha_{ij}^C + \alpha_{ij}^B + e_{BA}^{-1} \alpha_{ij}^A, \quad \tilde{\alpha} = e_{BC}^{-1} \alpha^C + \alpha^B + e_{BA}^{-1} \alpha^A \tag{17}$$

and

$$\begin{aligned}
\tilde{\eta}_{ij} &= e_{BC}^{-2} \eta_{ij}^C + \eta_{ij}^B + e_{BA}^{-2} \eta_{ij}^A \\
&+ e_{BA}^{-1} (\eta_{ij}^{BA} + \eta_{ij}^{AB}) + e_{BC}^{-1} (\eta_{ij}^{BC} + \eta_{ij}^{CB}) + e_{BA}^{-2} \cdot e_{AC}^{-1} (\eta_{ij}^{AC} + \eta_{ij}^{CA}), \\
\tilde{\eta} &= e_{BC}^{-2} \eta^C + \eta^B + e_{BA}^{-2} \eta^A \\
&+ e_{BA}^{-1} (\eta^{BA} + \eta^{AB}) + e_{BC}^{-1} (\eta^{BC} + \eta^{CB}) + e_{BA}^{-2} \cdot e_{AC}^{-1} (\eta^{AC} + \eta^{CA})
\end{aligned} \tag{18}$$

respectively.

2.2 1D Expression for three-scale problem

One-dimensional constitutive equation employed in this study is,

$$\dot{\gamma} = D_1 \{1 + c_1 \operatorname{sgn}(\tilde{\eta}) \sqrt{|\tilde{\eta}|}\} \ln(1 + c_2 \gamma) \quad (19)$$

where D_1, c_1, c_2 are constants. This is a reduced version of the constitutive equation for a crystalline plasticity model presented in section 4 of Part I, i.e.,

$$\dot{\gamma}^{(\alpha)} = f\left(\frac{\tau^{(\alpha)}}{K^{(\alpha)}}\right) \quad (20)$$

with

$$\dot{K}^{(\alpha)} = Q_{\alpha\beta} H(\gamma) |\dot{\gamma}^{(\alpha)}| \quad \text{and} \quad d_{cell} = k \left(\frac{1}{N} Q_{\alpha\beta} Q_{\alpha\beta} \right)^{-\frac{1}{2}} \quad (21)$$

where $H(\gamma)$ represents hardening modulus for a referential stress-strain curve, and $Q_{\alpha\beta}$ indicate hardening ratio further given as,

$$Q_{\alpha\beta} = \delta_{\alpha\beta} \{1 + F(\eta^{(\beta)})\} \quad (22)$$

with

$$F(\tilde{\eta}^{(\alpha)}) = \operatorname{sgn}(\tilde{\eta}^{(\alpha)}) \cdot \frac{k}{p_\eta} \cdot \left(\frac{l_{defect}}{b} |\tilde{\eta}^{(\alpha)}| \right)^{1/2} \quad (23)$$

Eq. (19) is evaluated, in the present study, from a given initial strain distribution that has been obtained in the FE analysis on multi-grained model (Aoyagi *et al.* 2008) and interpolated based on RKPM (See Fig. 1). In the present case, the scale B is set to be the reference, so the total incompatibility in the interaction field representation is written as,

$$\tilde{\eta} = e_{BC}^{-2} \tilde{\eta}_C + \tilde{\eta}_B + e_{BA}^{-2} \tilde{\eta}_A \quad (24)$$

Substituting Eq. (19)₂ into the above, we finally have,

$$\tilde{\eta} = e_{BC}^{-2} \eta_C + e_{BC}^{-1} \eta_{BC}^{int} + \tilde{\eta}_B + e_{BC}^{-2} \cdot e_{CA}^{-1} \eta_{BA}^{int} + e_{BA}^{-2} \tilde{\eta}_A + e_{BA}^{-1} \eta_{CA}^{int} \quad (25)$$

For the scale A in the 1D case, the effective cell size model is used to evaluate the strain distribution and its derivatives, assuming the periodicity commensurate with $d_{cell}(x)$ for the strain, instead of its tensorial counterparts given in Eq. (1), namely,

$$\gamma_A^p \equiv \gamma_{A0}^p \sin\left(\frac{2\pi}{d_{cell}(x)} x^A\right) \quad (26)$$

Here,

$$\tau = K\mu \frac{b}{d_{cell}(x)} = \mu \gamma^{cell} \Rightarrow \gamma^{cell} = \frac{Kb}{d_{cell}(x)} \quad (27)$$

where K is the proportionality constant. For the scales B and C, direct differentiations based on the central finite difference scheme are utilized with respect to the respective evaluation ranges, Δx^B and Δx^C .

$$\eta_B(x_i) = \nabla_B^2 \gamma_B^p \text{ and } \eta_C(x_i) = \nabla_C^2 \gamma_C^p \quad (28)$$

Similarly, for the interaction terms between scales B and C, we have,

$$\begin{cases} \eta_{BC}^{int}(x_i) = \nabla_B \nabla_C \gamma_C^p = \nabla_B \alpha_C \\ \eta_{CB}^{int}(x_i) = \nabla_C \nabla_B \gamma_B^p = \nabla_C \alpha_B \end{cases} \quad (29)$$

where the derivatives are evaluated also based on finite difference method, i.e., central difference for the spatial derivative and forward difference for the time derivative, i.e.,

$$\bar{\nabla}_B \gamma_B^p \equiv \frac{(\gamma_B^p)_{i+\Delta x_B/2} - (\gamma_B^p)_{i-\Delta x_B/2} - \{(\gamma_C^p)_{i+\Delta x_C/2} - (\gamma_C^p)_{i-\Delta x_C/2}\}}{\Delta x_B - \Delta x_C}, \nabla_C \gamma_B^p \equiv \frac{(\gamma_B^p)_{i+\Delta x_C/2} - (\gamma_B^p)_{i-\Delta x_C/2}}{\Delta x_C} \quad (30)$$

and

$$\nabla_B \alpha_C \equiv \frac{(\alpha_C)_{i+\Delta x_B/2} - (\alpha_C)_{i-\Delta x_B/2}}{\Delta x_B}, \nabla_C \alpha_B \equiv \frac{(\alpha_B)_{i+\Delta x_C/2} - (\alpha_B)_{i-\Delta x_C/2}}{\Delta x_C} \quad (30)'$$

For the scale A, the incompatibility is obtained by the second derivative of Eq. (26), i.e.,

$$\eta_A(x_i) = \nabla_A^2 \gamma_A^p = -\gamma_{A0}^p \left(\frac{2\pi}{d_{cell}} \right)^2 \sin\left(\frac{2\pi}{d_{cell}} x_i \right) \quad (31)$$

Therefore, the interaction terms become,

$$\begin{cases} \eta_{BA}^{int} = -\nabla_B \alpha_A(x_i) = \frac{\pi \gamma_{A0}^p}{d_{cell} \Delta x^B} \left\{ \cos\left(\frac{2\pi}{d_{cell}} x_{i+1}^B \right) - \cos\left(\frac{2\pi}{d_{cell}} x_{i-1}^B \right) \right\} \\ \eta_{AB}^{int} \cong \bar{\nabla}'_A \left\{ (-\alpha_B) \sin\left(\frac{2\pi}{\Delta x^B} x_i \right) \right\} = (-\alpha_B) \frac{2\pi}{\Delta x^B} \cos\left(\frac{2\pi}{\Delta x^B} x_i \right) \end{cases} \quad (32)$$

and

$$\begin{cases} \eta_{CA}^{int} = -\nabla_C \alpha_A(x_i) = \frac{\pi \gamma_{A0}^p}{d_{cell} \Delta x^C} \left\{ \cos\left(\frac{2\pi}{d_{cell}} x_{i+1}^C \right) - \cos\left(\frac{2\pi}{d_{cell}} x_{i-1}^C \right) \right\} \\ \eta_{AC}^{int} \cong \nabla_A \left\{ (-\alpha_C) \sin\left(\frac{2\pi}{\Delta x^C} x_i \right) \right\} = (-\alpha_C) \frac{2\pi}{\Delta x^C} \cos\left(\frac{2\pi}{\Delta x^C} x_i \right) \end{cases} \quad (33)$$

respectively.

3. Application example

Here we consider steels in fatigue focusing on the effect of dislocation substructures to be evolved during cyclic deformation. It has been shown experimentally (Yokoi *et al.* 2004) that steels yielding well-developed 3D cell structure of dislocations exhibit extrusion/intrusion at the specimen surface with the corresponding width to the average cell size of the order of sub-micro to micrometer ultimately leading to crack initiation from thereabout. By way of sharp contrast, steels yielding 2D substructures, i.e., that with vein or planer morphology, tend to be accompanied by finer extrusions at the sample surface that can significantly delay the crack initiation in comparison with the former case. Furthermore, the cyclic properties are also changed drastically from cyclic hardening to softening.

The above is a striking example of the multiscale properties observed in a certain class of steels that definitely needs to be interpreted and solved from “multiscale” perspective as in the present study. Note that those drastic changes in the dislocation substructures and the concomitant fatigue properties are reported to be caused by addition of copper depending on its form within the ferrite matrix, e.g., solid solution and nano-sized precipitates (Yokoi *et al.* 2004). The connection with the electronics, i.e., ab initio-based viewpoints and approach, has been extensively discussed separately elsewhere (Chen *et al.* 2008), where the addition of copper atoms is shown to drastically change the core structure of a screw dislocation of BCC iron from non-polarized to fully-polarized.

4. Analytical results and discussion

4.1 Results

Three scales, A, B and C, are considered as an example case of the application; each being assumed to be corresponding to the scale levels of dislocation substructures (A), crystal grains (B) and their aggregate (C), respectively. The characteristic scales commensurate with the respective evaluation size of the derivative operations set here are (A) 0.5, (B) 1.76 and (C) 8.8 μm , respectively, as depicted in Fig. 2. Therefore, the scale ratios for the present case are,

$$e_{BC}^{-1} = \frac{l_C}{l_B} = 5, \quad e_{BA} = \frac{l_A}{l_B} = 0.28, \quad e_{BA}^{-2} \cdot e_{AC}^{-1} = \frac{l_C l_A}{l_B^2} = 2.5 \quad (35)$$

In what follows, a use is made of the incompatibility terms for the individual scales A, B and C, together with the pair interactions between arbitrary two scale levels, i.e., BC, BA and AB. Here, they are evaluated separately via,

$$F(\eta^{scale}) \equiv \text{sgn}(\eta^{scale}) \sqrt{e_{scale} \cdot |\eta^{scale}|} \quad (36)$$

where “scale” indicates the distinction of scales, e.g., $scale = A$ for scale A and $scale = BC$ for inter-scale of B and C, etc, while e_{scale} expresses the corresponding scale ratio, e.g., e_{BA}^{-2} , e_{BA}^{-1} , e_{BA} , e_{AC}^{-1} , etc.

Fig. 4 displays thus obtained distributions for the respective incompatibility terms, i.e., individual-scale incompatibility and interaction terms. The scale A exhibits finer fluctuations than the others extending both positive and negative values reflecting the wavelength of the underlying effective

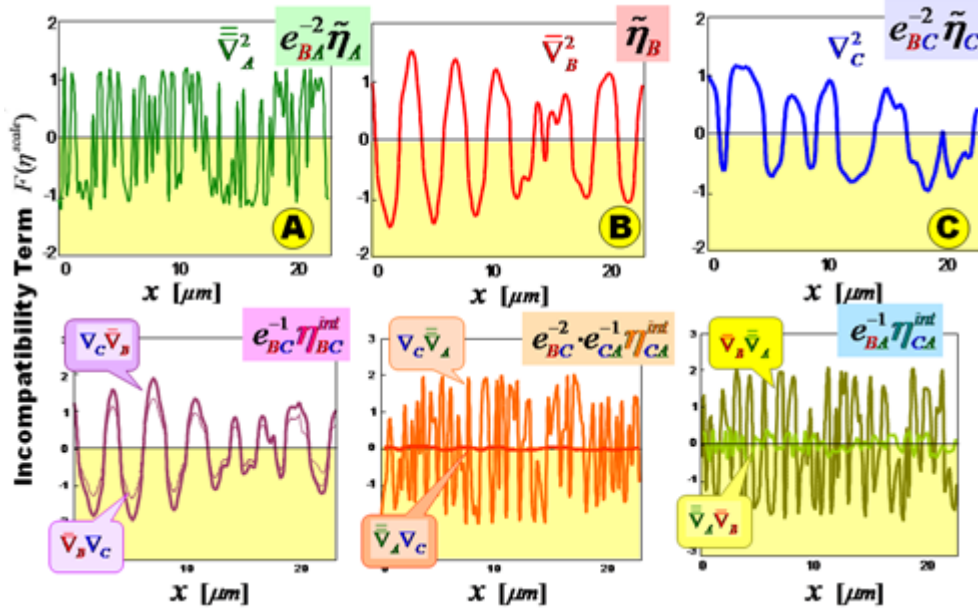


Fig. 4 Obtained incompatibility terms for A, B and C scales together with interaction terms

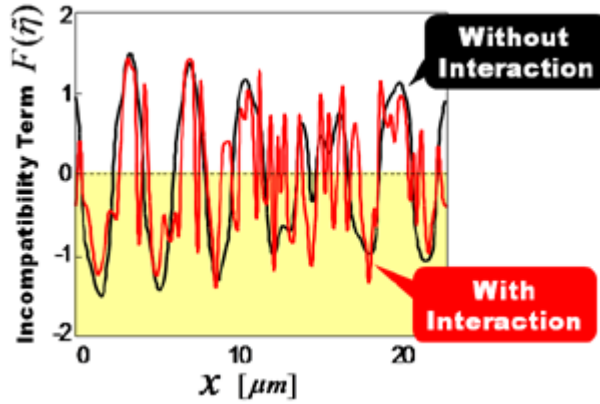


Fig. 5 Comparison of total incompatibility term distribution between with and without interaction

cell size $d_{\text{cell}}(x)$. The scales B and C show similar distribution to each other. Their interaction terms, BC and CB, yield slight difference between the two, which is caused by artificially introduced information loss in the differentiation operations (Eqs. 29 and 29') for the purpose of meeting the present aim. Large asymmetry, on the other hand, is observed in the interaction terms for the A-B and A-C scale pairs, i.e., $\eta_{BA}^{\text{int}} \gg \eta_{AB}^{\text{int}}$ and $\eta_{CA}^{\text{int}} \gg \eta_{AC}^{\text{int}}$. In the latter two cases, the A-scale fluctuation in the strain tends to be averaged out during the differentiation process with respect to the larger scale, i.e., B or C.

Fig. 5 shows the total incompatibility distribution $F(\tilde{\eta})$ for the interaction field comparing with that without interaction (referred to as ‘referential’). It is shown that the field interactions evidently enhance the total field fluctuation where finer modulations are superimposed on the referential field.

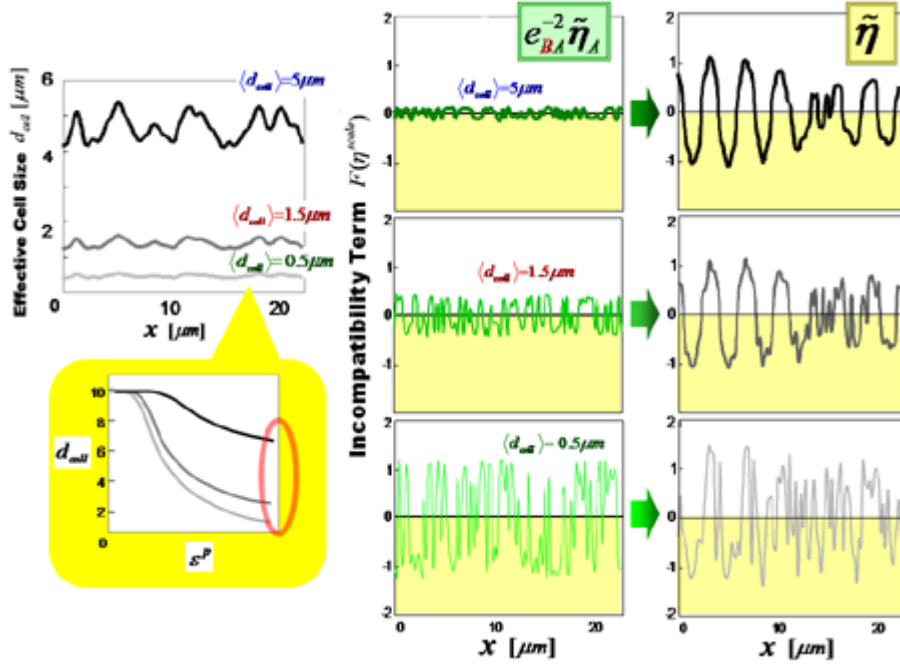
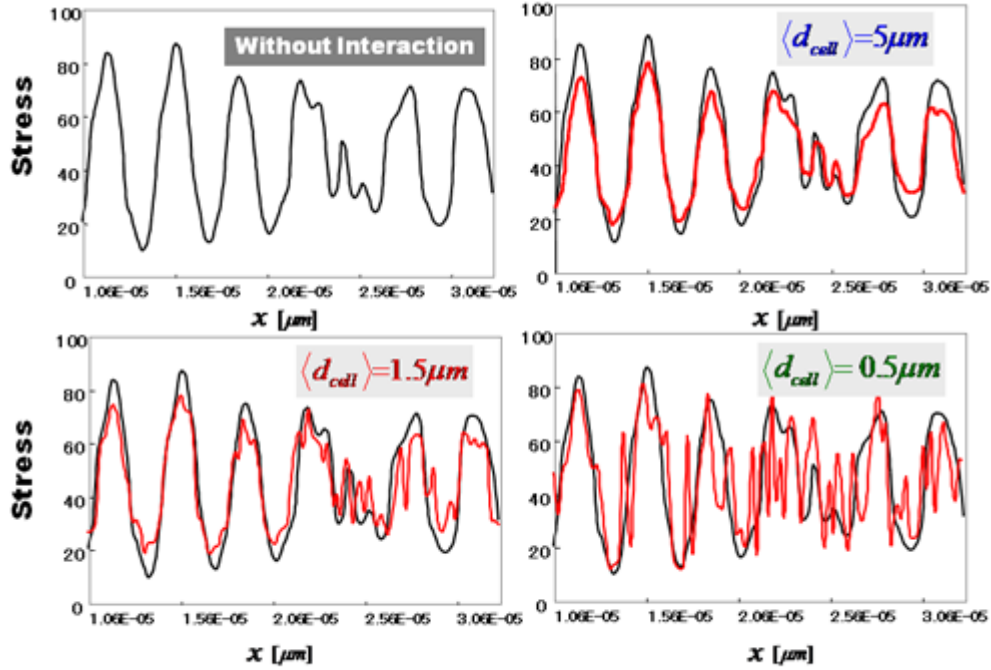


Fig. 6 Effect of A-scale fluctuation on total incompatibility distribution; (a) cell size distributions with three average sizes, (b) corresponding incompatibility term distributions for A scale and (c) resultant total incompatibility distributions comparing three cases

In the present case, as can be understood from the comparison among the results displayed in Fig. 4, the contribution from the A scale plays a prominent role especially through the interaction terms $F(\eta_{BA}^{int})$ and $F(\eta_{CA}^{int})$. This implies the importance of the field fluctuations in the dislocation substructure order in evaluating mesoscopic damage evolution, e.g., ultimately leading to crack initiation in fatigue. It must be emphasized that such microscopic information normally tends to be averaged out in the upper scale simulation based on conventional crystal plasticity.

Let us scrutinize further the effect of A-scale fluctuation on the interaction field. We consider three cases with different average sizes of the effective cell $d_{cell}(x)$ mimicking three distinct dislocation substructures to be evolved during high cycle fatigue, e.g., (1)three-dimensionally well-organized cell, (2)two-dimensionally developed vein and (3)uniformly distributed planer array of dislocations. These are assumed here to be modeled by introducing small, intermediate and large effective cell sizes, respectively, in the present context i.e., $\langle d_{cell} \rangle = 0.5, 1.5$ and $5 \mu\text{m}$. The latter two cases, for simplicity, employ the same $d_{cell}(x)$ distribution as the first one but multiplied by magnification factors with the amplitude leaving d_{cell} constant. Fig. 6(a) compares thus assumed cell size distributions with the three $\langle d_{cell} \rangle$, where the result for $\langle d_{cell} \rangle = 0.5 \mu\text{m}$ was obtained in the FE analysis in Aoyagi *et al.* (2008).

Fig. 6(b) shows comparison of the A-scale incompatibility term $F(\eta^A) = \text{sgn}(\eta^A) \sqrt{|\eta^A|}$ obtained for the three $\langle d_{cell} \rangle$ cases, while Fig. 6(c) displays the resultant total incompatibility terms $F(\tilde{\eta})$. It is clearly demonstrated that the difference in $\langle d_{cell} \rangle$ sensitively controls the fluctuation levels in the A-scale field, ultimately influencing those in the total incompatibility field. The largest cell size, i.e., $\langle d_{cell} \rangle = 0.5 \mu\text{m}$, brings about minute fluctuation in $F(\eta^A)$ with small enough amplitude, resulting



Part II- Fig.7

Fig. 7 Comparison of stress distribution among different interaction conditions in terms of average cell size in scale A

in the negligible effect on the total incompatibility $F(\eta^A)$, while the smallest size, i.e., $\langle d_{cell} \rangle = 0.5 \mu m$, causes larger and finer field fluctuations which significantly modulate the $F(\tilde{\eta})$ distribution especially in its frequency. The average size of $\langle d_{cell} \rangle = 0.5 \mu m$, on the other hand, exhibits the intermediate trends both in $F(\eta^A)$ and $F(\tilde{\eta})$ between the above two cases. These results demonstrate relatively high sensitivity of the A-scale field fluctuation to the overall response in terms of field fluctuation.

Corresponding stress distributions to the above total incompatibility are compared in Fig. 7, demonstrating the noticeable effect of $\langle d_{cell} \rangle$ also on the resultant fluctuation in the stress field. Significantly enhanced fluctuations can be observed, where the small enough $\langle d_{cell} \rangle$ evidently makes the stress field further modulated with respect to the scale of the order of $\langle d_{cell} \rangle$ keeping the overall distribution profile unaltered. The large enough $\langle d_{cell} \rangle$, in sharp contrast, results in much smaller and, accordingly, negligible effect on it. Also we can notice that the amplitude of the averaged response is slightly reduced with increasing contribution of the A-scale field fluctuation. This is due to the additional degrees of freedom in deformation to accommodate the imposed inhomogeneity which tends to soften the stress response as mentioned in Part I (Hasebe 2008).

Practically, the above results for the stress response with enhanced fluctuation is expected to be closely related with rougher surface undulations, e.g., during fatigue (e.g., Yokoi, *et al.* 2004). Therefore, we can conclude that the introduction of the interaction field among multiple scales captures the essential effects of the microscopic fluctuations, e.g., those in the dislocation substructure order, normally absent in the conventional crystal plasticity-based models and

simulations, on the inhomogeneous field evolutions in the upper scales, which will be macroscopically averaged out.

Note, below the scale A, dynamical effects associated with moving and interacting individual dislocations are expected to become dominant, generating “temporal” field fluctuations rather than or in addition to the “spatial” fluctuations discussed above, whose contribution can in principle be taken into account by combining separate and direct simulations based on, e.g., dislocations dynamics (Kubin *et al.* 1992, Zbib *et al.* 1998, Ghoniem *et al.* 1999). An example of related discrete dislocation-based discussion on the effect of stress field fluctuation on the stability of dense dislocation structures is found in Yamada *et al.* (2008).

5. Toward system stability/instability evaluation

One of the ultimate scopes of the present study is to develop a novel methodology to be able to evaluate the stability/instability of the complex systems of polycrystalline materials in plasticity, explicitly considering interactions among multiple scales accompanied by evolving inhomogeneous fields. In this section, a candidate framework will be presented based on the interaction field formalism given above.

In the interaction field theory, everything about the field evolution is characterized by

$$[F(\tilde{\boldsymbol{\eta}})] = \begin{bmatrix} F(e_{BC}^{-2}\boldsymbol{\eta}^C) & F(e_{BC}^{-1}\boldsymbol{\eta}^{CB}) & F(e_{BA}^{-2} \cdot e_{AC}^{-1}\boldsymbol{\eta}^{CA}) \\ F(e_{BC}^{-1}\boldsymbol{\eta}^{BC}) & F(\boldsymbol{\eta}^B) & F(e_{BA}^{-1}\boldsymbol{\eta}^{BA}) \\ e_{BA}^{-2} \cdot e_{AC}^{-1} F(\boldsymbol{\eta}^{AC}) & e_{BA}^{-1}F(\boldsymbol{\eta}^{AB}) & F(e_{BA}^{-2}\boldsymbol{\eta}^A) \end{bmatrix} \equiv \begin{bmatrix} F_C^\eta & F_{CB}^\eta & F_{CA}^\eta \\ F_{BC}^\eta & F_B^\eta & F_{BA}^\eta \\ F_{AC}^\eta & F_{AB}^\eta & F_A^\eta \end{bmatrix} \quad (37)$$

which is further introduced in the incompatibility term of the hardening model. A preliminary analysis will be made by utilizing the above matrix, which is called “evolutionary matrix” hereafter. Each component in the evolutionary matrix is tentatively evaluated by a signed spatial average, i.e.,

$$F_{scale}^\eta \equiv \text{sgn} \left\{ \sum_{\omega}^N F(\eta_B^{(\omega)}) \right\} \sqrt{\frac{1}{N} \sum_{\omega}^N |F(\eta_B^{(\omega)})|^2} \quad (38)$$

The evolution of the system will be virtually simulated by a continued product of the evolutionary matrix wong time, and is evaluated via a phase diagram, i.e., $F_{scale}^\eta - \dot{F}_{scale}^\eta$, where

$$[F_{scale}^\eta]_n \equiv [F_{scale}^\eta]^n - [F_{scale}^\eta]^{n-1} \quad (39)$$

From the results shown in Fig. 4, we have,

$$[F_{scale}^\eta] = \begin{bmatrix} -8.7 & -7.5 & 13.0 \\ -7.0 & 6.5 & -3.0 \\ -2.2 & -0.12 & -8.8 \end{bmatrix} \quad (40)$$

The above matrix is asymmetric and cannot be diagonalized. The corresponding phase diagram with reference to the scale B, i.e., $F_B^\eta - \dot{F}_B^\eta$, is displayed in Fig. 8(a). Variations of F_B^η and \dot{F}_B^η with power n is shown in Fig. 8(b). Oscillation takes place initially and is followed by limit cycle-like

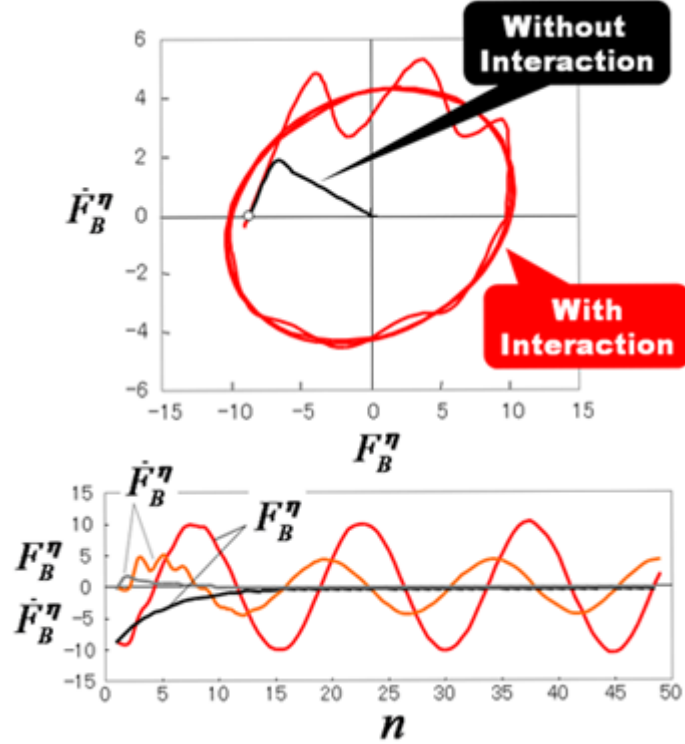


Fig. 8 Results of a virtual system stability analysis based on evolutionary matrix comparing cases with and without field interactions. (a) Phase diagram, i.e., F_B^η vs. \dot{F}_B^η and (b) variations of F_B^η and \dot{F}_B^η with number of simulation steps

behavior as n increases. This implies that the system will oscillate in the B scale order as cyclic deformation proceeds.

Let us next examine some virtual cases with different off-diagonal terms. If there is no interaction, all the off-diagonal components should vanish, i.e.,

$$[F_{scale}^\eta] = \begin{bmatrix} -8.7 & 0 & 0 \\ 0 & 6.5 & 0 \\ 0 & 0 & -8.8 \end{bmatrix} \quad (41)$$

This case corresponds to a system composed of linearly interacted and thus completely separable multiple scales, with no unpredictable response. The discriminant of the characteristic equation in this case is $D_{discr} = -22.0 < 0$ meaning the equation have three distinct real roots. The phase diagram and variations of F_B^η and \dot{F}_B^η for this case are also shown in Fig. 8(a) and (b), respectively. No limit cycle-like oscillation takes place in this case, and a convergence is reached soon, implying that the system is stable in the absence of field interaction.

Several other examples have been examined based on the slightly modified evolutionary matrices from Eq. (40). Variations as spiral converging, spiral diverging, and zigzag behavior on the phase diagram are observed depending on the difference in the off-diagonal components. These results imply that even with slight differences in the off-diagonal components can result in totally different

system response. Possibilities of chaotic responses will be pursued in the next step. Also it should be noted that the above is just a “toy” problem of a preliminary kind. The full 3D polycrystalline systems may exhibit totally different and more complex responses, since the scales B and C have qualitatively different incompatibility field in terms of the distribution and evolution based on its origin as exemplified previously. Further details of these results will be presented in the next study.

6. Conclusions

This paper applied the mathematical formalism for describing multiple field interactions constructed in Part I to a three-scale problem assuming a multi-grained plasticity of steels under fatigue, where three orders of dislocation substructures (A), grain size (B) and grain aggregates (C) were considered. A one-dimensional constitutive model together with plastic strain distribution obtained in FEM-RKPM (reproducing kernel particle method) analysis was used for the simulation. Field fluctuations both for individual scales and the interaction terms were explicitly obtained and their roles on the evolution of the overall system were discussed. In the present context, the A-scale fluctuations were demonstrated to be highly influential in the upper scale field evolutions, especially in the scale B, which is consistent with experimentally reported results. Furthermore, a candidate scope for the system stability analysis was proposed based on an evolutionary matrix to be evaluated from the incompatibility distributions.

References

- Aoyagi, Y. and Hasebe, T. (2007), “New physical interpretation of incompatibility and application to dislocation substructure evolution”, *Key Engineering Materials*, **340-341**, 217-222.
- Aoyagi, Y., Hasebe, T., Chen, J.-S. and Guan, P.-C., “Reproducing kernel based evaluation of incompatibility tensor in field theory of plasticity”, *Interaction and Multiscale Mechanics, An Int. J.*, **1**(4).
- Chen, J.S., Pan, C., Wu, C.T. and Liu, W.K. (1996), “Reproducing kernel particle methods for large deformation analysis of nonlinear structures”, *Comput. Methods Appl. Mech. Eng.*, **139**, 195-227.
- Chen, Z.Z., Kioussis, N., Ghoniem, N. and Hasebe, T. (2008), “Lubricant effect of copper nano-clusters on dislocation core in α -Fe”, *Physical Review B.*, **77**-1, 014103.
- Ghoniem, N.M. and Sun, L.Z. (1999), “Fast-sum method for the elastic field of three-dimensional dislocation ensembles”, *Phys. Rev.* **B60**, 128-140.
- Ghoniem, N.M., Tong, S.-H. and Sun, L.Z. (1999), “Parametric dislocation dynamics: A thermodynamics-based approach to investigations of mesoscopic plastic deformation”, *Phys. Rev.* **B61**, 913-927.
- Hasebe, T., Kumai, S. and Imaida, Y. (1999), “Impact behavior of FCC metals with pre-torsion strains”, *Mater. Process. Technol.*, **85**, 184-187.
- Hasebe, T. (2004a): “Continuum description of inhomogeneously deforming polycrystalline aggregate based on field theory”, *Mesosopic Dynamics of Fracture Processes and Materials Strength (Proc. IUTAM Symp.)*, Eds. H. Kitagawa, Y. Shibutani, Kluwer, 381-390.
- Hasebe, T. (2004b), “Field theoretical multiscale polycrystal plasticity”, *MRS-J*, **29**(8), 3619-3624.
- Hasebe, T. (2006), “Multiscale crystal plasticity modeling based on field theory”, *CMES*, **11**(3), 145-155.
- Hasebe, T. (2009), “Field theory-based description of interaction field for multiple scales: Part I-theory-”, *Interaction and Multiscale Mechanics*, **2**(1), 1-14.
- Kubin, L.P., Canova, G., Condat, G., Devincere, B., Pontikis, V. and Brechet, Y. (1992), “Dislocation microstructures and plastic flow: 3D simulation”, *Solid State Phenomena*, **23 & 24**, 455-472.
- Liu, W.K., Jun, S. and Zhang, Y.F. (1995), “Reproducing kernel particle methods”, *Int. J. Numer. Methods*

- Fluids*, **20**, 1081-1106.
- Phillips, R. (2001), *Crystals, Defects and Microstructures, Modeling Across Scales*, Cambridge.
- Yamada, M., Hasebe, T., Tomita, Y. and Onizawa, T. (2008), "Dislocation dynamics simulation on stability of high dense dislocation structure interacting with coarsening defects", *Interaction and Multiscale Mechanics*, **1**(4).
- Yokoi, T., Takahashi, M., Maruyama, N. and Sugiyama, M. (2004), "Application of controlled Cu nano-precipitation for improvement in fatigue properties of steels", *Nippon Steel Technical Report*, **381**, 45-50 (in Japanese).
- Zbib, H.M., Rhee, M. and Hirth, J.P. (1998), "On plastic deformation and the dynamics of 3D dislocations", *Int. J. Mech. Sci.*, **40**, 113-127.